Effects of increased CO_2 levels on monsoons

Annalisa Cherchi[1], Andrea Alessandri[2], Simona Masina[1], and Antonio Navarra[1]

[1]Centro Euro-Mediterraneo per i Cambiamenti Climatici, and Istituto Nazionale di Geofisica e Vulcanologia, Bologna, Italy
[2]Centro Euro-Mediterraneo per i Cambiamenti Climatici, Bologna, Italy

Manuscript Accepted on

Climate Dynamics

DOI: 10.1007/s00382-010-0801-7 13/03/2010

Abstract

Increased atmospheric carbon dioxide concentration provided warmer atmospheric temperature, higher atmospheric water vapor content, but not necessarily more precipitation. A set of experiments performed with a state of the art coupled general circulation model (CGCM) forced with increased atmospheric CO_2 concentration (two, four and sixteen times the present-day mean value) have been analyzed and compared with a control experiment to evaluate the effect of increased CO_2 levels on monsoons. Generally, the monsoon precipitation responses to CO_2 forcing are largest if extreme concentrations of carbon dioxide are used, but they are not necessarly proportional to the forcing applied. In fact, despite a common response in terms of atmospheric water vapor increase to the atmospheric warming, two out of the six monsoons studied simulate less or equal summer mean precipitation in the 16xCO2 experiment compared to the intermediate sensitivity experiments. The precipitation differences between CO_2 sensitivity experiments and CTRL have been investigated specifying the contribution of thermodynamic and purely dynamic processes. As a general rule, the differences depending on the atmospheric moisture content changes (thermodynamic component) are large and positive, and they tend to be damped by the dynamic component associated with the changes in the vertical velocity. However, differences are observed among monsoons in terms of the role played by other terms (like moisture advection and evaporation) in shaping the precipitation changes in warmer climates. The precipitation increase, even if weak, occurs despite a weakening of the mean circulation in the monsoon regions ("precipitation-wind paradox"). In particular, the tropical east-west Walker circulation is reduced, as found from velocity potential analysis. The meridional component of the monsoon circulation is changed as well, with larger (smaller) meridional (vertical) scales.

1 Introduction

In the most recent decade, the global mean concentration of carbon dioxide and the atmospheric radiative forcing associated to it experienced the largest change within the last two centuries (Forster et al., 2007). Changed atmospheric radiative forcing alters the atmospheric heating distribution and its hydrological cycle. The atmospheric moisture content rise in response to global warming is constrained by the Clausius-Clapeyron (C-C, hereinafter) relationship, but the rate of precipitation increase as predicted by the climate models is slower (Allen and Ingram, 2002; Held and Soden, 2006; Richter and Xie, 2008). The so-called "suppressant effect of CO_2" implies that the changes in the turnover of the hydrologic cycle are controlled by the availability of energy rather than by the availability of moisture (Boer, 1993; Allen and Ingram, 2002). Model results including climate future scenarios show that rainfall tends to increase in convergence zones with large climatological precipitation and to decrease in subsidence regions ("rich-get-richer" mechanism; Chou and Neelin, 2004; Held and Soden, 2006). However, within convergence zones dynamic feedbacks may substantially increase or decrease the precipitation anomalies (Chou et al., 2009) and mechanisms involving for example increased or decreased ascent have to be addressed.

In the tropical continents, the largest portion of rainfall during the year is provided by the summer monsoons, occurring as a seasonal reverse of the mean circulation in response to land-sea thermal contrast (Webster, 1987). The identification of the differences among the tropical monsoons favoured separated studies and communities for each monsoon domain. Recent efforts have been dedicated to the research of common aspects between them, for example in the study of the diurnal cycles (Lau et al, 2007), up to the introduction of the concept of a global monsoon with specific metrics (Wang and Ding, 2008; Zhou et al., 2008).

In order to explore the response of the monsoon climate to atmospheric warming, possibly identifying differences in the individual monsoon dynamics, we classified the monsoon domains in boreal and austral monsoons, depending on their occurrence in the Northern or in the Southern Hemisphere summer, respectively. During the boreal summer, the Northern Hemisphere is interested by three main monsoon systems: the South Asian summer Monsoon (SAM), the West African Monsoon (WAM) and the North American Monsoon (NAM). The broad-scale South Asian summer monsoon consists of separated entities differing both in climatology and variability because of different land-ocean configurations and topographic forcing (Murakami and Matsumoto, 1994; Wang et al., 2005). Here we divided it into two parts: the Indian Summer Monsoon (ISM, as the portion west of 100°E) and the East Asian Summer Monsoon (EASM, including the region east of

100°E and expanding to the subtropics). On the other hand, the austral summer is characterized by the Australian Monsoon (AuM) and the South American Monsoon System (SAMS). The skeleton of the above classification is coherent with Meehl (1992), where the characteristics of the various monsoons have been described in terms of topographic and orographic structures.

To study the effect of increased CO_2 levels on monsoons we used a set of experiments with CO_2 multiplied by a factor of two, four and sixteen with respect to present-day mean value. A recent analysis of the same set of experiments revealed the possibility to have decreased precipitation in the Tropical Western Pacific as a response to an increased lower and upper tropospheric stability triggered by a positive feedback between surface temperature and clouds (Cherchi et al., 2008). The non-linearity in terms of the mean global climate response to atmospheric forcing found in the most extreme experiment may give hints in the understanding of the changes in the monsoon thermodynamics. The changes occurring in the monsoon regions due to increased CO_2 levels are analyzed in terms of the atmospheric moisture equation following the idea that the precipitation is mostly balanced by a thermodynamic component driven by changes in the water vapor and a dynamic component associated with changes in the mean circulation (Emori and Brown, 2005; Chou et al., 2009). The contribution from the moisture content change tends to be uniform in space (Chou et al., 2009), hence we expect to have more informations on the monsoon regional behaviour from the dynamic component. Another aspect in the relationship between precipitation and mean circulation is the precipitation increase despite a weakened atmospheric circulation ("precipitation-wind paradox"; Ueda et al., 2006). In order to understand the importance of the issue for each monsoon we analyzed the zonal mean circulation components in terms of mean potential velocity and we discussed the meridional overturning in the monsoon areas.

The study is organized as follows: section 2 describes the model and the experiments used in the analysis, and it lists the observational and re-analysis datasets used for comparison with the model results. Section 3 describes the methodology chosen including the classification and the domains of the monsoons considered. Section 4 contains the main results of the study organized into three different subsections to describe i) the mean hydro-climate response to carbon dioxide increase; ii) the moisture equation terms for each monsoon and iii) the analysis of the relationship between precipitation and atmospheric circulation. Finally, section 5 summarizes the main conclusions.

2 Model simulations and data

The experiments analyzed in this study have been performed using SINTEXG (Gualdi et al., 2008), a fully coupled atmosphere-ocean general circulation model with interactive sea-ice. It represents a recent upgrade of the SINTEX CGCM (Gualdi et al., 2003) with the ocean model coupled to a thermodynamic sea-ice model.

The atmospheric component is ECHAM4.6 with a T30 horizontal resolution, corresponding to $3.75^\circ \times 3.75^\circ$ grid points, and 19 vertical sigma levels. The radiation scheme is a narrow-band-model described and validated in Morcrette (1984) and Morcrette and Fouquart (1985). Despite the high concentration of carbon dioxide considered, the scheme has been found to be robust and free from saturation. More details about the physics and dynamics of the atmospheric component may be found in Roeckner et al. (1996). The oceanic component is the primitive equation model OPA8.2. The distribution of the variables is over a three-dimensional Arakawa-C-type grid, with a spatial resolution of about $2^\circ \times 2^\circ$ and a meridional refinement of 0.5° at the Equator, and 31 prescribed vertical levels (Madec et al., 1998).

Four experiments have been used for the analysis. A rather long (300 years of integration) control experiment (CTRL) has been compared with a set of experiments with atmospheric carbon dioxide concentration (mass mixing ratio equivalent to 353 ppmV) multiplied by a factor of 2, 4 and 16 obtaining 2xCO2, 4xCO2 and 16xCO2 experiments, respectively. More details about the experiments analyzed and the coupled model used may be found in Cherchi et al. (2008).

The summer mean climate has been compared with observations and atmospheric re-analysis datasets. In particular, the observed precipitation field comes from the CMAP dataset (Xie and Arkin, 1997), while the wind fields is taken from the NCEP reanalysis (Kalnay et al, 1996).

3 Monsoon classification and methodology

As mentioned in the introduction, we will focus on six monsoons, classified as boreal (Indian Summer Monsoon, ISM; East Asian Summer Monsoon, EASM; West African Monsoon, WAM and North American Monsoon, NAM) and austral (Australian Monsoon, AuM and South American Monsoon System, SAMS). Table 1 summarizes them, specifying their regional bounds and the season used for the averages of the thermodynamic variables analyzed in section 4.

The thermodynamic variables used in the analysis of the atmospheric water vapor content balance are tropospheric vertically integrated specific humidity (qvi), that is a proxy for the tropospheric vertically integrated water vapor content, relative humidity averaged in the troposphere up

to 200 mb (RH, computed as described in appendix A) and horizontal moisture flux convergence ($-\nabla Q$). In fact, the water vapor content in the atmosphere is a balance between the water fluxes at the lower boundary interface and the horizontal moisture flux convergence. The equation for the atmospheric water vapor content may be written as:

$$\frac{\partial W}{\partial t} + \nabla \cdot Q = E - P \tag{1}$$

where W is the amount of water vapor contained in a unit area atmospheric column, Q is the vertically integrated (from the Earth's surface to the top of the atmosphere) horizontal transport of water vapor, E is the evapotranspiration and P is the precipitation (Peixoto and Oort, 1992).

A further step in the analysis of the vertically integrated moisture budget is done in terms of the precipitation departures from the CTRL simulation, following the analysis published by Chou et al. (2009):

$$P^{'} = -\langle \overline{\omega} \partial_p q^{'} \rangle - \langle \omega^{'} \partial_p \overline{q} \rangle - \langle v \cdot \nabla q \rangle^{'} + E^{'} + q_{res} \tag{2}$$

where prime represents the difference from the CTRL, and the overbar denotes the climatology in the CTRL experiment. The angle brackets stand for vertically integrated quantities through the troposphere. E is the evaporation, ω is pressure velocity, v is the horizontal velocity and q is the specific humidity (in W/m^2 by absorbing the latent heat per unit mass L). The first term on the right-hand side of equation 2 represent the thermodynamic precipitation change (Chou et al., 2009) and we will identify it as the q-term. The second term corresponds to a dynamic precipitation change and we identify it as ω-term, while the third term is the horizontal advection term. The residual term identified as q_{res} contains the contribution of the non-linear components, e.g. $-\langle \omega^{'} \partial_p q^{'} \rangle$.

4 Results

4.1 Summer mean climate response to CO_2 increase

Figure 1 shows the precipitation difference between JJA and DJF, indicating the position of the dominant monsoon domains as positive (negative) patterns for the Northern (Southern) Hemisphere. In the CMAP dataset, the positive values in the Northern Hemisphere evidence the precipitation maxima associated with the broad-scale Asian summer monsoon (in the domain 60°-130°E), the West African monsoon (20°W-40°E) and the North American (125°-95°W) monsoon. On the other hand, the negative values in the Southern Hemisphere are indicative of the DJF peaks over

North Australia and South America associated with the Australian monsoon (AuM) and the South American Monsoon System (SAMS), respectively.

The coupled model is able to reproduce the basic features of the precipitation patterns (fig. 1b). The performance of SINTEX in the simulation of the Asian summer monsoon has been extensively described by Cherchi and Navarra (2007). Here we just point out that the simulated precipitation are weaker than observed over India, in the Bay of Bengal and in the Western North Pacific sector. The existence of an oceanic monsoon system over the Western North Pacific was first introduced by Murakami and Matsumoto (1994) from annual OLR differences.

Over West Africa, the coupled model produces stronger than observed precipitation (fig. 1b). The bias in the precipitation pattern is strictly associated with the low-level wind simulation. In particular, in the West African continent between the Equator and 10°N low level winds blow north-easterly over the continent and mainly easterly in the equatorial Atlantic Ocean (not shown). The simulated low-level winds in the Equatorial Atlantic Ocean are stronger than observed and they have a larger north-westerly component linked to an Equatorial Atlantic Ocean thermocline slope reversed with respect to the observations (not shown). The last bias is a systematic error common to many coupled models which complicates the performance of WAM simulations (Thorncroft and Lamb, 2005). In the Southern Hemisphere, the model has stronger than observed precipitation over both North Australia and South America (fig. 1b). In the south-western Pacific Ocean, the simulated DJF max has a dominant east-west feature rather than north-south as in the observations. This bias is associated with the systematic error of the model in reproducing a double ITCZ, as many other CGCMs (e.g. de Szoeke and Xie, 2008; Lin, 2007; Bellucci et al., 2009).

Rainfall over the SAM domain globally intensifies as the CO_2 increases (fig. 1c,d,e), consistently with some previous modelling studies (Meehl and Washington, 1993; May, 2004; Annamalai et al., 2007). However, a recent high resolution regional model study evidenced a reduction of Indian monsoon rainfall associated with anthropogenic increases in greenhouse gas concentrations (Ashfaq et al., 2009), thus suggesting that there are still great uncertainties for projecting the South Asian summer monsoon precipitation. On the other hand, the response of WAM precipitation to CO_2 increase is non-linear: in 2xCO2 and 4xCO2 experiments the precipitation increases in the western part of the continent (fig. 1c,d), while in the 16xCO2 experiment the positive values are lower than in the intermediate experiments, indicating a rainfall decrease (fig. 1e). African summer rainfall and Indian summer monsoon are not independent (Camberlin, 1997; Liu and Yanai, 2001, among others) and their responses to CO_2 forcing may result from changes to the whole Eurasia-African monsoon circulation. In the Southern Hemisphere, in both northern Aus-

tralia and south America the simulated summer mean precipitation is stronger as the atmospheric CO_2 increases (fig. 1c,d,e).

Summer monsoon precipitation is associated with the seasonal reverse in the circulation pattern. Over Asia, an index of the monsoon dynamic is the zonal wind vertical shear (U850-U200, Webster and Yang, 1992). There, the magnitude of the regional vertical shear is in fact highly related with the strength of the heating (Webster, 1972; Gill, 1980). In the Northern Hemisphere summer, the max U850-U200 are localized in a zonal band with a peak at 10°N covering South Asia, West Africa and North America monsoon domains. Hence it is reasonable to take a meridional average between 5°S and 15°N to evaluate the model performance and its response to CO_2 increase (fig. 2). The coupled model simulates in a realistic way the position of the shear maxima, but the intensity is weaker than observed. In both the South Asian and North America domains the shear progressively weakens as the CO_2 increases. On the other hand, in the West African domain the shear slightly increases in 2xCO2 and 4xCO2 experiments, and then drastically decreases in the extreme case (fig. 2). In the Southern Hemisphere summer the maxima associated with both the Australian monsoon and the South American Monsoon System are less pronounced (not shown).

For the Asian summer monsoon, increased monsoon rainfall despite weakened monsoon winds- ("precipitation-wind paradox", Ueda et al., 2006) has been ascribed to larger moisture flux convergence due to the enhancement of the moisture transport from a warmer Indian Ocean toward the Indian continent. In our sensitivity experiments, the atmospheric vertically integrated specific humidity is always larger than in the control experiment in both boreal and austral summer (fig. 3 and fig. 4, respectively). Over Asia the moisture flux from the Indian Ocean becomes larger as the atmospheric CO_2 increases: in 16xCO2 experiment the difference from the CTRL is about eight times the values of the 2xCO2 case (fig. 3a,c). For the Indian sector, a larger transport of moisture toward the continent is accomplished by stronger atmospheric winds blowing northward. In fact, in the lower troposphere the south westerly flow intensify (not shown), competing with the weakening of the vertical shear (fig. 2). Similar findings have been discussed in previous studies (e.g. May, 2004; Ueda et al., 2006; Annamalai et al., 2007). In the other boreal monsoon domains, the increase of moisture flux is less pronounced (fig. 3) and other mechanisms rather than increased moisture transport have to be addressed. Over West Africa, in the 16xCO2 experiment, positive vertically integrated specific humidity differences are superposed to negative precipitation differences (fig. 3c), as indicated by the position of the solid black line representing the zero-contour of the precipitation differences from the CTRL.

In the Southern Hemisphere summer (fig. 4) over the continents there is a correspondence be-

tween positive values of the precipitation and vertically integrated moisture content differences. For example, over South America the moisture transport from the Atlantic Ocean is increased in all the CO_2 experiment compared to the CTRL (fig. 4a,b,c). The moisture equation analysis described in section 3 will help to investigate the relative role played by the major terms involved in the precipitation changes.

4.2 Atmospheric moisture equation analysis

There is consensus among model results that for a given temperature difference, the atmospheric moisture content increase is much larger than the corresponding precipitation rate rise (Allen and Ingram, 2002; Held and Soden, 2006; Vecchi and Soden, 2007, among others). The issue is investigated here on a regional scale for the different monsoon domains evaluating the response of the atmospheric moisture terms to increased atmospheric forcing.

Fig. 5 shows the relationship between the atmospheric temperature (integrated from the ground up to 200 mb) rise, expressed as difference of CO_2 experiments results and CTRL values (ΔT, in K), and the thermodynamic atmospheric variables as defined in section 3, expressed as anomalous percentages of 2xCO2 (plus signs), 4xCO2 (filled circles) and 16xCO2 (filled squares) with CTRL (e.g. (P-P(CTRL))/P(CTRL), for the precipitation). All the variables shown in the figure have been averaged in the corresponding summer of the monsoon domains (see table 1 for details), each represented by a different color.

Comparing the monsoon domains considered, the relationship between atmospheric temperature increase (in K) and tropospheric vertically integrated water vapor content (qvi) change is of the same order (fig. 5a), with a huge increase in 16xCO2 experiment (about 250% larger than in the CTRL). In 2xCO2 and 4xCO2 experiments where the temperature changes range from 2 to 8°C, the values may fit a 7.5% increase per 1 K of temperature warming (fig. 5a). However, when the temperature changes become much larger, e.g. 20°C for the 16xCO2 experiment cases, the moisture changes are not supposed to fit the same line, being the C-C relationship non-linear (see Appendix A).

The relationship evidenced in fig. 5a is expected from an increase in vapor pressure under the assumption of a constant global relative humidity (Vecchi and Soden, 2007). Actually, a constant relative humidity (RH) constraint is supposed to be valid for the global mean, but it is not uniform in space (Dai, 2006; Sun et al., 2007). Generally, the changes occurring in RH as the atmospheric temperature increases are small (fig. 5b), reflecting some proportionality between the expected increased water holding capacity of the atmosphere and the simulated atmospheric water vapor

content. In particular, in 2xCO2 experiment the RH increase is below 5% for all the regions considered. The largest RH increases occur in the Asian-Australian domain for both 4xCO2 and 16xCO2 experiments, with differences around 8-10% and 12-18%, respectively (fig. 5b).

Over the monsoon regions, the precipitation rate increase is weaker than the associated atmospheric vertically integrated moisture content rise (fig. 5c), in agreement with the so-called "suppressant effect of CO_2" (Allen and Ingram, 2002; Held and Soden, 2006; Ueda et al., 2006; Vecchi and Soden, 2007; Richter and Xie, 2008). Under their assumptions, the changes in the hydrologic cycle may rely on the ability of the troposphere to radiate away the latent heat released by precipitation (Allen and Ingram, 2002). On the global average, the precipitation change for a given temperature increase is held because the global precipitation is constrained by global energy balance, while on the regional scale this energy constraint is not necessarly satisfied. In our sensitivity experiments the precipitation increase is always lower than the 7.5% increase per 1 K warming (blue solid line, fig. 5c), rather it better corresponds to a 1.7% increase per 1 K warming (dashed black line, fig. 5c), as found by Held and Soden (2006), at least in the intermediate experiments. In 16xCO2 results, where the largest differences occur, two of the six regions of this study reflect a non-linear response of the precipitation rate to atmospheric warming (fig. 5c). In fact, WAM and NAM experience a weaker increase of precipitation in the 16xCO2 experiment compared to the intermediate experiments. On the other hand, the Asian-Australian domain (ISM, EASM and AuM) has an almost monotonic relationship between temperature and precipitation changes (fig. 5c). Actually, despite the temperature increase for all the monsoon domains considered is very similar, the associated precipitation rate change is highly variable, suggesting that the dynamic component of the moisture convergence becomes more important.

The relationship between precipitation rate and moisture flux convergence changes is shown in fig. 5d. In this case the moisture flux convergence differences are expressed as percentages over the mean precipitation of the CTRL simulation (e.g. $[(-\nabla Q(\text{2xCO2}))\text{-}(-\nabla Q(CTRL))]/P(CTRL)$ for the 2xCO2 case). The moisture convergence differences are weighted on the CTRL precipitation to be sure that the anomalous percentage is an effective measure of the relative contribution of the moisture convergence to the precipitation for each monsoon region. A clear linear response of the precipitation rate to the applied atmospheric forcing would imply little change in the corresponding circulation. The non-linear response, on the other hand, should be related to changes in the circulation. In most of the intermediate CO_2 cases, a large increase of moisture flux convergence occurs and it is converted into a precipitation increase (fig. 5d). Rather, all the points away from the red line (y=x) are indicative of atmospheric moisture content that is not converted

into precipitation (fig. 5d). The cases far from the line (e.g. the values in most of the 16xCO2 cases, colored squares) are indicative either of decreased evaporation or of an increase of the water vapor remaining in the atmospheric column. In 16xCO2 experiment, WAM has a peculiar behaviour as the moisture flux convergence reduces and the precipitation increase is lower than in the intermediate experiments.

At this point the application of the decomposition of the precipitation differences described in section 3 is important to highlight the contribution of moisture content changes (q-term), circulation impact (ω-term and advection) and evaporation changes, eventually identifying differences from monsoon to monsoon, as suggested by fig. 5d.

Fig. 6 and 7 show the horizontal maps of the thermodynamic component (q-term in equation 2) of the precipitation change computed from the CO_2 sensitivity experiments for boreal and austral summer, respectively. The q-term depends on the changes occurring to the atmospheric moisture content and it is considered the thermodynamic component (Emori and Brown, 2005; Chou et al., 2009). As shown in figs. 6 and 7 it tends to be large and positive within the convergence zones, that can be identified inside the zero-contour of the summer mean vertical velocity at 500 mb, shown by a black solid line in the figures.

On the other hand, the vertical dynamic component (ω-term in equation 2) may be positive or negative within the convergence zone and even within the same monsoon region (fig. 8 and fig. 9). Actually, in the convergence zones, positive precipitation anomalies may be associated with both enhanced or reduced tropical circulation (Chou et al., 2009). In our experiments, the contribution from the vertical dynamic component seems to be weaker than the thermodynamic contribution, as the values of fig. 8 and 9 are lower than in fig. 6 and 7. Further, when the ω-term is negative it acts to reduce the precipitation change compared to the moisture increase (fig. 8 and fig. 9).

Over Asia (for both ISM and EASM) the q-term change is always positive as the atmospheric carbon dioxide concentration increases (fig. 6). Conversely, the ω-term is positive over both Southern India and Northern India, while it is negative over central India and eastern China (fig. 8). A similar conclusion can be drawn for the other boreal monsoons: over West Africa and North America the precipitation change due to the q-term is positive and progressively larger as the atmospheric carbon dioxide increases (fig. 6), while that associated to the ω-term tends to be negative, particularly for the whole NAM region and for the western part of Africa (fig. 8). Actually over Africa in the 16xCO2 experiment, the negative values extend from the western edge to the whole region (fig. 8c). Even in the case of the austral monsoon the q-term is always positive, while the ω-term tends to be negative and highly variable in space (figs. 7 and 9).

However, the precipitation changes described from fig. 1 and fig. 5 can not be completely explained by the combination of thermodynamic and vertical velocity terms. In fact, in our sensitivity experiments both the moisture advection and the evaporation differences may significantly contribute to the changes occurring to the precipitation. To understand the different mechanisms acting in each monsoon domain, the individual terms of the equation 2 are analyzed in the different areas. Fig. 10 shows the equation terms, as fraction of P', for each monsoon domain. Generally, the results of 2xCO2 and 4xCO2 experiments have a common behaviour within the same region, whilst the 16xCO2 outputs may be completely different (fig. 10). The thermodynamic component is positive and it constitutes the largest contribution (always more than 50%) to the precipitation increase in all the monsoons (fig. 10). In most of the cases, the thermodynamic contribution would be even larger than 1, but it is damped out by the other terms. In the figure, the term identified as residual in equation 2 is included to evidence that its influence to the precipitation change is not negligible.

Over India, the precipitation increase in the intermediate CO_2 experiments is the sum of positive values of q-term, ω-term and evaporation, and a negative contribution from the moisture advection change (fig. 10a). A similar behaviour is found for West Africa (fig. 10c) and for North America (fig. 10d), though in the latter case the evaporation term has a positive contribution in 4xCO2 experiment but not in 2xCO2 experiment. Further, the three monsoons have a complete different response in the extreme CO_2 experiment. In fact, in 16xCO2 experiment over India the large positive q-term is damped out by all the other terms, including the evaporation. In the ISM the dynamic precipitation change is negative because the vertical velocity difference is positive (weakening of ascent) in 16xCO2, differently from the other two cases where it is negative. Over North America the response of each terms remains of the same sign as in the intermediate experiments, but each contribution is magnified. In particular, a huge increase of precipitation due to direct moisture effect is suppressed by a huge decrease of the moisture advection (fig. 10d) because of the large weakening of the atmospheric wind shear both in zonal and meridional directions (not shown). For the West African monsoon the contributions of the ω-term and the q-term in 2xCO2 and 4xCO2 experiments are comparable and both positive, like for NAM. For both the systems, in the 16xCO2 experiment the contribution of all terms is drastically larger than in the other cases.

Over East Asia (fig. 10b) in the intermediate CO_2 experiments a contribution of the q-term larger than one is mostly damped by the evaporation changes. Over South America the largest differences from the CTRL occur in 4xCO2 experiment (fig. 10f). The q-term is balanced primarily by the moisture advection reduction due to the weakening of the meridional wind intensity

(not shown). Over Australia, the thermodynamic effect, the larger evaporation available and the non-linear components of equation 2 contribute positively to the precipitation changes (fig. 10e).

Summarizing, fig. 10 shows that the monsoon systems may be organized into two categories: ISM, AuM and EASM where the contribution of the q-term clearly dominates and WAM, NAM and SAMS where vertical velocity changes and horizontal advection of moisture are equally important. Within the last group, two systems (WAM and NAM) have a peculiar response in 16xCO2 experiment. In fact, in these two cases the differences are many times larger than in the CTRL. At this point we may not exclude that the large response of WAM and NAM in the extreme CO_2 experiment depend on the model used and on the experiments design. Nevertheless, WAM and NAM can be identified as outliners in most of the analysis described and they present a clear non-linear response, e.g. in terms of precipitation difference, to the increased atmospheric CO_2 concentration. We may speculate that in WAM and NAM the response may strongly depend on the distinct role played by evaporation (fig. 10) and by moisture flux convergence (fig. 5) in the moisture budget.

4.3 Weakening of the monsoon circulation

The precipitation increase discussed in the previous subsection occurs despite an apparent weakening of the atmospheric wind, as mentioned in the discussion of fig. 2. Recent studies revealed that atmospheric warming due to anthropogenic forcing might induce a weakening of the atmospheric zonal and meridional circulations in the tropics (Lu et al., 2007; Vecchi and Soden, 2007). The weakening of the zonal atmospheric circulation is associated to large-scale east-west overturning of air across the Pacific Ocean (Walker circulation) that reduced in recent decades and in climate model projections of future climate (Vecchi et al., 2006). On the other hand, in the meridional direction an increased subtropical static stability is supposed to cause an expansion of the Hadley cell, reducing its intensity and pushing poleward the baroclinic instability (Lu et al., 2007).

From the results of the previous section, we have been able to discuss how the changes in the circulation, in terms of horizontal advection and vertical velocity, may contribute to a significant portion of the precipitation change in most of the monsoon considered. In the following, the monsoon circulation will be investigated by means of velocity potential and meridional overturning analysis.

The tropical east-west circulation differences have been analyzed by means of the velocity potential (χ) at 200 mb. Fig. 11 (12) shows the JJA (DJF) mean differences of velocity potential and divergent wind at 200 mb for 2xCO2, 4xCO2 and 16xCO2 experiments with respect to

CTRL. Areas with positive anomalies are indicative of intensification of subsidence, while the negative anomalies are associated with intensified ascending motion. In fact, the anomalous convergent/divergent inflow/outflow in the upper troposphere may be associated with anomalous ascending or descending midtropospheric motion (not shown). Over Asia in both JJA for the South Asian domain (fig. 11) and DJF for the AuM (fig. 12) the divergence is remarkably reduced, indicating a weakened monsoon circulation. Over India and East Asia the vertical velocity differences in the mid-troposphere indicate a weakened ascent of motion from the intermediate to the extreme CO_2 experiments (not shown). In 16xCO2 experiment in JJA, the Walker circulation type is further reduced, with weakened Asian monsoon circulation and intensified upward motion in the Eastern Pacific Ocean (fig. 11c).

In the other monsoons (WAM, NAM and SAMS) the velocity potential differences are negative and indicate an intensification of the upward motion (fig. 11 for WAM and NAM, and fig. 12 for SAMS). Over West Africa, the differences over the continent are negative in 2xCO2 and 4xCO2 experiments, indicating a strengthening of the ascending motion and then become positive in the western edge of the continent in 16xCO2 experiment (fig. 11a,b,c). In fact, as shown in fig. 10 the contribution of the integrated vertical velocity is positive in the intermediate experiments while it become negative in the 16xCO2 experiment.

The different changes in the strength of the summer monsoon circulations, i.e. weakened for the Asian-Australian monsoons and strengthened for WAM, NAM and SAMS, may imply a weaker change in the globally averaged meridional circulation, i.e. the Hadley.

In terms of atmospheric overturning circulation, from a global point of view, the poleward extension of tropical rain-band is associated with the edge of the meridional Hadley circulation (Seidel et al., 2008). Surface zonal wind (or eventually the streamfunction at 500 mb) may be used as metric for the identification of the position of the Northern edge of the Hadley cell (Lu et al., 2007). In our experiments the computation of the edge of the Hadley cell identified by the transition latitude from zonal mean surface easterlies to westerlies moves from 28°N in the CTRL to 29.5° in 16xCO2. However, the resolution of the model used is too coarse (3.75° $\times$ 3.75° horizontal resolution grid) to assign significance to the latitudinal shift found. In terms of intensity, the annual mean mass streamfunction reveals a weakening (i.e. the maxima reduce by about 10% in 2xCO2 and 4xCO2 experiments, and by about 25% in 16xCO2 experiment) of both north and south poleward subtropical branches as the atmospheric CO_2 increases (not shown).

Locally, each monsoon area is interested by an overturning circulation with ascending and descending motions that can be represented in terms of meridional streamlines. Comparing the

solutions in each monsoon domain, it is possible to identify a general rule corresponding to a reduction (intensification) of the vertical (meridional) scale. A clear example of this behaviour is the ISM (fig. 13). Over India (60°-90°E), the overturning cell becomes wider as the atmospheric carbon dioxide concentration increases, and in the vertical the maximum of the overturning moves downward, in agreement with a most stable atmospheric column (fig. 13).

The changes discussed in the overturning circulation may influence the latitudinal distribution of the precipitation shifting meridionally the monsoon rain-band. In our sensitivity experiments it is hard to identify a significant shift of the latitudinal position of the precipitation maxima in the monsoon areas but some differences may be discussed. Fig. 14 shows the summer mean precipitation averaged in the monsoon longitudes (see table 1 for the details) for each monsoon (in the band 10°S-40°N for the NH monsoons and 40°S-10°N for the SH ones) and for each experiment. In the 16xCO2 experiment (green line) the precipitation values are huge compared to CTRL (black line) in those monsoon where the direct moisture effect dominates (e.g. ISM, AuM and EASM). Over India the position of the precipitation maxima moves slightly northward with reduced precipitation over the ocean and larger precipitation over the continent (fig. 14a). Over East Asia, Northern Australia and South America the precipitation profiles tend to widen without a real shift in the position of the maxima (fig. 14b,e,f).

5 Conclusions

All monsoon areas experience a huge increase of atmospheric vertically integrated specific humidity when the atmospheric carbon dioxide concentration is increased in 2xCO2, 4xCO2 and 16xCO2 climate simulations. In fact, according to the Clausius-Clapeyron relationship, warmer atmospheric temperature favour increased atmospheric water holding capacity. However, the precipitation rate increase is smaller than the moisture content rise, consistently with the so-called "suppressant effect of CO_2" described by Allen and Ingram (2002) and found in scenario simulations for the global climate (Held and Soden, 2006; Richter and Xie, 2008, among others).

The precipitation differences between the CO_2 sensitivity experiments and a CTRL simulation have been decomposed into terms, following the analysis of Chou et al. (2009), thus allowing the distinction of the contributions of moisture content change, mean circulation effect (both horizontal and vertical) and evaporation differences.

Generally, the dominant player to the precipitation changes in all the experiments with respect to the CTRL simulation is the q-term (thermodynamic component), i.e., the term that depends on

the water vapor content changes. The ω-term (vertical velocity change), the horizontal moisture advection and the evaporation play different roles case by case. The thermodynamic component tends to have a uniform character, being large and positive in the convergence zones, while the vertical velocity component is highly variable in space and tends to damp the precipitation increase. The contribution of the advection term in damping the precipitation increase may be as large as the contribution of the vertical velocity component. In summary, the monsoons may be organized into two categories with a group where the direct moisture effect clearly dominates (ISM, AuM and EASM) and the others where the vertical velocity changes and the horizontally advection of moisture are equally important (WAM, NAM and SAMS).

The precipitation increase may occur despite a weakened atmospheric circulation, actually the weakening of the monsoon circulation is responsible for a precipitation increase smaller than what expected from a direct moisture effect. Over Asia, we evidenced that in our experiments the tropical east-west circulation is reduced, and that the divergence at 200 mb is remarkably weaker in CO_2 experiments compared to the CTRL, while upward motion intensify in the eastern Pacific. Despite this weakening, the monsoon of the Pacific/Indian sector (ISM, AuM and EASM) experience a precipitation increase mostly driven by a huge increase in the atmospheric moisture content. On the other hand, for WAM, NAM and SAMS the velocity potential differences at 200 mb indicate an intensification of the upward motion. Locally, the meridional overturning in the monsoon areas is characterized by a weakening of the vertical scale, as for example over India the mid-tropospheric maximum moves downward in warmer conditions. On the other hand, it is possible to identify an intensification in the meridional direction, with the dominant cell becoming wider as in the case of the ISM.

The differences among the monsoons precipitation response may be characterized even in terms of proportionality of the response to CO_2 forcing. Over West Africa and North America the precipitation change in 16xCO2 experiment is comparable or even lower than in the intermediate sensitivity experiments. In our model, these two monsoons are the only ones in which precipitation changes in the extreme CO_2 experiment are explained by a compensation of very high changes in all the terms of the budget. Conversely, the Indian summer monsoon experiences a large moisture flux convergence and precipitation increase. In this region an increased moisture transport is responsible of the precipitation increase despite a weakened circulation (see also Ueda et al., 2006).

The issue of the proportionality of the climate response to CO_2 forcing has been widely discussed in the previous study analyzing the same set of experiments but focusing on the tropical

sector and on the tropical Pacific variability (Cherchi et al., 2008). With the results found in the present study we may extend the discussion to the mechanisms working in the monsoons. In fact, non-linear differences have been found in the subset of monsoons where the changes in CO_2 sensitivity experiments compared to a control simulation were mainly related to the vertical velocity and horizontal moisture advection variations. Both of them, in fact, may not be strictly proportional to the atmospheric moisture increase driven by increased atmospheric temperature: the former because of its dependence on purely dynamic processes, the latter because of its dependence on the meridional circulation.

Despite the individual complexities of the monsoons considered we have been able to apply a common analysis and to identify important differences in terms of the response to the carbon dioxide forcing applied. The classification drawn according to the monsoon response to increased atmospheric CO2 forcing, both in terms of precipitation and circulation, separate the phenomena into two groups depending on the processes at work in driving the changes (i.e. purely thermodynamic or purely dynamic processes, or horizontal moisture advection variations). In the present climate, the above classification corresponds to the distinction between the strongest and likely classical monsoons (i.e. ISM, EASM, AuM, or the Asian-Australian monsoons) and the weaker ones (i.e. WAM, NAM and SAMS), thus emphasizing the importance of the differences in the monsoon dynamic and its possible consequences. A detailed analysis of the implications of our results for the present-day climate monsoons would require precise attention, but it is well beyond the scope of the present study. The results presented here may be largely model dependent, but, when comparable, they have been strengthen by previous numerical studies.

Acknowledgements. This work has been done in the "Numerical Application and Scenarios" division of CMCC in the framework of the activity "Understanding of the climate system". We are grateful to the anonymous reviewers whose comments greatly improved the analysis and to C Cagnazzo for her advises related to radiative issues arised. A Cherchi thanks GA Vecchi and H Annamalai for useful discussion and suggestions in the preliminary part of the study.

Appendix A Computation of the relative humidity

The relative humidity as a measures of the balance between the water holding capacity of the atmosphere and the tropospheric water vapor content has been computed by means of the formula:

$$RH = \frac{q}{q_s} * 100 \tag{A1}$$

where q is the specific humidity (in g/kg) and q_s is the saturation specific humidity. The saturation specific humidity may be approximated as a function of the saturation vapor pressure e_s and of the atmospheric pressure p through

$$q_s \simeq 0.622 \frac{e_s}{p} \tag{A2}$$

where 0.622 is the ratio of the gas constant of dry air and of water vapor (R_d/R_v). The saturation vapor pressure can be expressed as a function of temperature only, by means of empirical formulae, e.g.:

$$e_s \simeq 6.11 \times 10^{\frac{7.5T}{237.7+T}} \tag{A3}$$

where T is the temperature expressed in °C (Bolton, 1980). RH has been computed from the surface up to 200 mb and then averaged in the tropospheric column.

References

Adams DK, Comrie AC (1997) The North American Monsoon. Bull Am Meteor Soc 78: 2197–2213

Allen MR, Ingram WJ (2002) Constraints on future changes in climate and the hydrologic cycle. Nature 419: 224–232

Annamalai H, Hamilton K and Sperber KR (2007) The South Asian summer monsoon and its relationship with ENSO in the IPCC AR4 simulations. J Climate 20 1071-1092

Ashfaq M, Shi Y, Tung WW, Trapp RJ, Gao XJ, Pal JS, Diffenbaugh NS (2009) Suppression of south Asian summer monsoon precipitation in the 21st century. Geophys Res Lett 36: L01704 doi:10.1029/2008GL036500

Bellucci A, Gualdi S, Navarra A (2009) The double-ITCZ syndrome in coupled general circulation models: the role of large-scale vertical circulation regimes. J Clim DOI: 10.1175/2009JCLI3002.1

Boer GJ (1993) Climate change and the regulation of the surface moisture and energy budgets. Clim Dyn 8:225–239

Bolton D (1980) The computation of equivalent potential temperature. Mon Wea Rev 108: 1046–1053

Camberlin P (1997) Rainfall Anomalies in the Source Region of the Nile and Their Connection with the Indian Summer Monsoon. J Clim 10: 1380–1392

Cherchi A, Navarra A (2007) Sensitivity of the Asian summer monsoon to the horizontal resolution: differences between AMIP-type and coupled model experiments. Clim Dyn 28: 273–290

Cherchi A, Masina S and Navarra A (2008) Impact of extreme CO_2 levels on tropical climate: A CGCM study. Clim Dyn 31: 743–758

Chou C, Neelin JD (2004) Mechanisms of global warming impacts on regional tropical precipitation. J Clim 17:2688–2701

Chou C, Neelin JD, Chen C-A, Tu J-Y (2009) Evaluating the "rich-get-richer" mechanism in tropical precipitation change under global warming. J Climate 22: 1982–2005

Dai A (2006) Recent climatology, variability and trends in global surface humidity. J Climate 19: 3589–3606

de Szoeke SP, Xie SP (2008) The tropical eastern Pacific seasonal cycle: Assessment of errors and mechanisms in IPCC AR4 coupled ocean-atmosphere general circulation models. J Clim 21: 2573–2590

Emori S, Brown SJ (2005) Dynamic and thermodynamic changes in mean and extreme precipitation under changed climate. Geophys Res Lett 32 doi:10.129/2005GL023272

Forster P, Ramaswamy V, Artaxo P, Berntsen T, Betts R, Fahey DW, Haywood J, Lean J, Lowe DC, Myhre G, Nganga J, Prinn R, Raga G, Schulz M, Van Dorland R (2007) Changes in Atmospheric Constituents and in Radiative Forcing. In: Climate Change 2007: The Physical Science Basis. Contribution of Working Group I to the Fourth Assessment Report of the Intergovernmental Panel on Climate Change [Solomon S, Qin D, Manning M, Chen Z, Marquis M, Averyt KB, Tignor M, Miller HL (eds.)]. Cambridge University Press, Cambridge, United Kingdom and New York, NY, USA.

Gill AF (1980) Some simple solutions for heat induced tropical circulations. Quart J Roy Meteor Soc 106: 447–462

Gualdi S, E Scoccimarro and A Navarra (2008) Changes in Tropical Cyclone Activity due to Global Warming: Results from a High-Resolution Coupled General Circulation Model. J Climate 21 5204-5228

Gualdi S, Navarra A, Guilyardi E, Delecluse P (2003) Assessment of the tropical Indo-Pacific climate in the SINTEX CGCM. Ann Geophys 46: 1–26

Held IM, Soden BJ (2006) Robust responses of the hydrological cycle to global warming. J Clim 19: 5686–5699

Kalnay E, Kanamitsu M, Kistler R, and co-authors (1996) The NCEP/NCAR 40-Year Reanalysis Project. Bull Am Meteor Soc 77 437-471

Lau KM, Kim K-M and Lee M-I (2007) Characteristics of diurnal and seasonal cycles in global monsoon systems. J Meteor Soc Jpn 85A: 403–416

Lin JL (2007) The double-ITCZ problem in IPCC AR4 coupled GCMs: Ocean-atmosphere feedback analysis. J Clim 20: 4497–4925

Liu X, Yanai M (2001) Relationship between the Indian monsoon rainfall and the tropospheric temperature over the Eurasian continent. Quart J Roy Meteor Soc 127: 909–937

Lu J, Vecchi GA, Reichler T (2007) Expansion of the Hadley cell under global warming. Geophys Res Lett 34: L06085, doi:10.1029/2006GL028443

Madec G, Delecluse P, Imbard M, Levy C (1998) OPA version 8.1 Ocean General Circulation Model reference manual. Tech Rep LODYC/IPSL Note 11

May W (2004) Potential future changes in the Indian summer monsoon due to greenhouse warming: analysis of mechanisms in a global time-slice experiment. Clim Dyn 22: 389–414

Meehl GA (1992) Effect of tropical topography on global climate. Ann Rev Earth Planet Sci 20: 85–112

Meehl GA, Washington WM (1993) South Asian summer monsoon variability in a model with doubled atmospheric carbon dioxide concentration. Science 260: 1101-1104

Morcrette JJ (1984) Sur la paramétrisation du rayonnement dans le modèles de la circulation générale atmosphérique. Thèse de Doctorat d'Etat, Université de Sciences et Techniques de Lille, 630.

Morcrette JJ, Fouquart Y (1985) On systematic errors in parameterized calculations of longwave radiation transfer. Q J Roy Meteorol Soc 111: 691-708

Murakami T, Matsumoto J (1994) Summer monsoon over the Asian continent and Western North Pacific. J Meteor Soc Jpn 72:719–745

Peixoto JP and Oort AH (1992) Physics of climate. Am Inst of Physics 520 p

Richter I, Xie S-P (2008) Muted precipitation increase in global warming simulations: A surface evaporation perspective. J Geophys Res 113: D24118 doi:10.1029/2008JD010561

Roeckner E, Arpe K, Bengtsson L, Christoph M, Claussen M, Dümenil L, Esch M, Giorgetta M, Schlese U, Schulzweida U (1996) The Atmospheric general circulation Model ECHAM4: Model description and simulation of present-day climate. *Max-Planck Institut für Meteorologie*, Report no. 218, Hamburg, 86

pp.

Seidel DJ, Fu Q, Randel WJ, Reichler TJ (2008) Widening of the tropical belt in a changing climate. Nature Geoscience 1: 21–24

Sun Y, Solomon S, Dai A, Portmann RW (2007) How often will it rain? J Clim 20: 4801–4818

Thorncroft C and Lamb P (2005) The West African monsoon. WMO/TD no. 1266

Ueda H, Iwai A, Kuwako K, Hori ME (2006) Impact of anthropogenic forcing on the Asian summer monsoon as simulated by eight GCMs. Geophys Res Lett 33: L06703, doi:10.1029/2005GL025336

Vecchi GA, Soden BJ (2007) Global warming and the weakening of the tropical circulation. J Clim 20: 4316–4340

Vecchi GA, Soden BJ, Wittenberg AT, Held IM, Leetma A, Harrison MJ (2006) Weakening of tropical Pacific atmospheric circulation due to anthropogenic forcing. Nature 441: 73–76

Wang B, Ding Q (2008) Global monsoon: dominant mode of annual variation in the tropics. Dyn Atm Oc 44: 165–183

Wang B, Li T, Ding Y, Zhang R, Wang H (2005) East Asian-Western North Pacific Monsoon: a distinctive component of the Asian-Australian monsoon system. In: *The Global Monsoon System: Research and forecast* WMO/TD No.1266

Webster PJ (1972) Response of the tropical atmosphere to local steady forcing. Mon Wea Rev 100: 518–541

Webster PJ (1987) The elementary monsoon. In: *Monsoons* (J.S. Fein and P.L. Stephens Eds.) Wiley-Interscience

Webster PJ, Yang S (1992) Monsoon and ENSO: Selectively interactive systems. Quart J Roy Meteor Soc 118: 877–926

Webster PJ, Magana V, Palmer TN, Shukla J and co-authors (1998) Monsoons: processes, predictability and the prospects for prediction. J Geophys Res 103 14451-14510

Wu R (2008) Possible Role of the Indian Ocean in the In-Phase Transition of the Indian-to-Australian Summer Monsoon. J Clim 21: 5727–5741

Xie P and Arkin P (1997) Global precipitation: a 17-year monthly analysis based on gauge observations, satellite estimates, and numerical model outputs. Bull Am Meteor Soc 78 2539-2558

Zhou J, Lau KM (2001) Principal modes of interannual and decadal variability of summer rainfall over South America. Int J Climatol 21: 1623–1644

Zhou TJ, Yu RC, Li HM, Wang B (2008) Ocean forcing to changes in global monsoon precipitation over the recent half century. J Clim 21: 3833–3852

Tables

Table 1. List of the monsoon domains considered in the analysis, including name, acronym used in the text, domain and peak season for space and time averages of atmospheric variables and a reference paper.

NAME	ACRONYM	DOMAIN	SEASON	REFERENCE*
Indian Summer Monsoon	ISM	60°-90°E,5°-35°N	JJA	Webster et al. (1998)
East Asian Summer Monsoon	EASM	110°-160°E, 10°-50°N	JJA	Wang et al. (2005)
West African Monsoon	WAM	20°W-40°E, 5°-20°N	JJA	Thorncroft and Lamb (2005)
North American Monsoon	NAM	125°-95°W, 20°-45°N	JJA	Adams and Comrie (1997)
Australian Monsoon	AuM	100°-150°E, 20°S-5°S	DJF	Wu (2008)
South American Monsoon System	SAMS	80°-30°W, 25°S-10°N	DJF	Zhou and Lau (2001)

* Just one reference has been chosen for each domain.

Figure Captions

Fig. 1. JJA minus DJF mean precipitation (mm/day) computed from (a) CMAP dataset, (b) CTRL, (c) 2xCO2, (d) 4xCO2 and (e) 16xCO2 experiments.

Fig. 2. Mean JJA U850-U200 (m/s) averaged between 5°S-15°N for NCEP winds (dashed black line), CTRL (solid black line), 2xCO2 (red line), 4xCO2 (blue line) and 16xCO2 (green line) experiments.

Fig. 3. JJA mean tropospheric vertically integrated specific humidity (kg/m^2, shaded) and water vapor flux (kg m^{-1} s^{-1}, vectors) differences from CTRL for (a) 2xCO2, (b) 4xCO2 and (c) 16xCO2 experiments. To maintain a unique vector length and a unique palette for all the experiments, the values of 4xCO2 and 16xCO2 cases have been divided by 2 and 8, respectively. The thick black solid line is the zero-contour difference of summer mean precipitation between CO_2 experiments and CTRL.

Fig. 4. Same as fig. 3 but for DJF.

Fig. 5. Scatter plots of atmospheric temperature (T) differences versus (a) vertically integrated atmospheric water vapor content (qvi), (b) relative humidity (RH), (c) precipitation rate (P) anomalous percentages of 2xCO2 (crosses), 4xCO2 (filled circles) and 16xCO2 (filled squares) from CTRL in the different monsoon domains (red for ISM, cyan for EASM, green for WAM, blue for NAM, magenta for AuM, yellow for SAMS, black for SAfM). (d) is the scatter plot of precipitation anomalous percentages (ΔP), computed as described above, versus moisture flux convergence differences weighted on the precipitation of the CTRL ($\Delta(-\nabla \cdot Q)/P(CTRL)$ %). The solid blue line in panels (a) and (c) corresponds to a 7.5% increase per 1K warming, the dark dashed line in panel (c) corresponds to 1.7% increase per 1 K warming and the red line in panel (d) is y=x.

Fig. 6. JJA q-term ($-\langle\overline{\omega}\partial_p q^{'}\rangle$, mm/day) for (a) 2xCO2, (b) 4xCO2 and (c) 16xCO2 experiments with respect to CTRL. The thick solid line is the zero-contour of the summer mean vertical velocity at 500 mb, and it is used to delimit the convergence zones.

Fig. 7. Same as fig. 6 but for DJF.

Fig. 8. JJA ω-term ($-\langle\omega^{'}\partial_p\overline{q}\rangle$, mm/day) for (a) 2xCO2, (b) 4xCO2 and (c) 16xCO2 experiments with respect to CTRL. The thick solid line is the zero-contour of the summer mean vertical velocity at 500 mb, and it is used to delimit the convergence zones.

Fig. 9. Same as fig. 8 but for DJF.

Fig. 10. Moisture terms of equation 2 expressed as fraction of P' for each monsoon domain as 2xCO2 (blue), 4xCO2 (green) and 16xCO2 (dark red) differences from CTRL. The terms shown are 1 - precipitation difference (P'), 2 - q-term ($- < \overline{\omega}\partial_p q' >$), 3 - ω-term ($- < \omega'\partial_p \overline{q} >$), 4 - advection term ($- < v \cdot \nabla q >'$), 5 - evaporation change (E'), and 6 - residuals (q_{res}). Each term is averaged in the corresponding monsoon region (a) Indian subcontinent (ISM), (b) East Asia (EASM), (c) West Africa (WAM), (d) North America (NAM), (e) Northern Australia (AuM) and (f) South America (SAMS) following the details specified in table 1. The y-axis in (c) and (d) is larger than in the other cases.

Fig. 11. Velocity potential ($10^6 m^2 s^{-1}$, contours) and divergent wind (vectors) at 200 mb as JJA mean differences of (a) 2xCO2, (b) 4xCO2 and (c) 16xCO2 experiment from CTRL. Positive (negative) values are in red (blue) solid (dashed) lines and contour interval is 0.3, 0.5 and 1 10^6 $m^2 s^{-1}$ in 2xCO2, 4xCO2 and 16xCO2 experiment, respectively.

Fig. 12. Same as fig. 11, but for DJF.

Fig. 13. Streamlines of divergent and vertical velocity over India for (a) CTRL, (b) 2xCO2, (c) 4xCO2 and (d) 16xC02 experiments.

Fig. 14. Meridional profiles of summer mean rainfall (mm/day) zonally averaged over the monsoon areas of (a) ISM, (b) EASM, (c) WAM, (d) NAM, (e) AuM and (f) SAMS for CTRL (black), 2xCO2 (red), 4xCO2 (blue) and 16xCO2 (green) experiments.

Figures

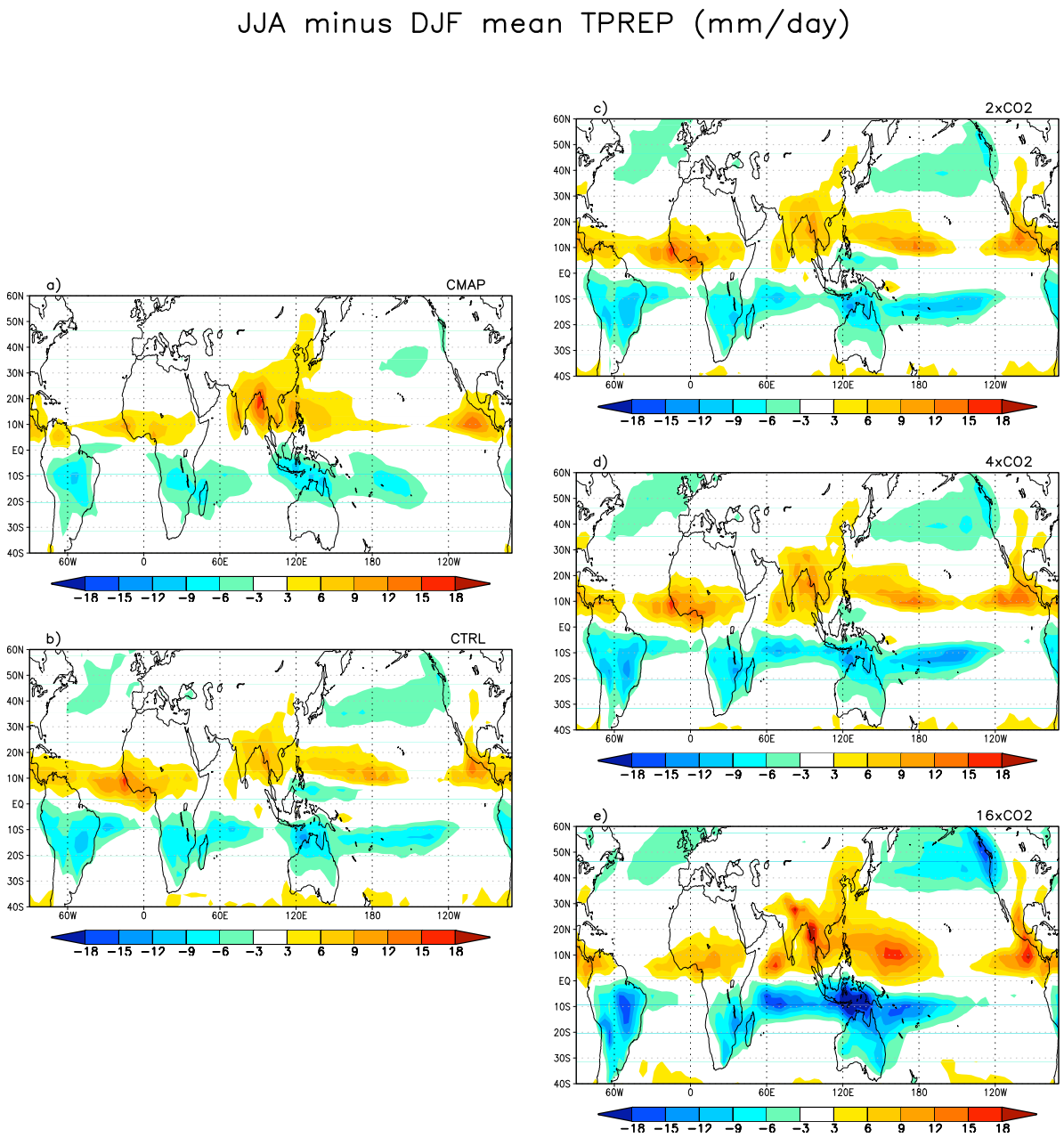

Fig. 1. JJA minus DJF mean precipitation (mm/day) computed from (a) CMAP dataset, (b) CTRL, (c) 2xCO2, (d) 4xCO2 and (e) 16xCO2 experiments.

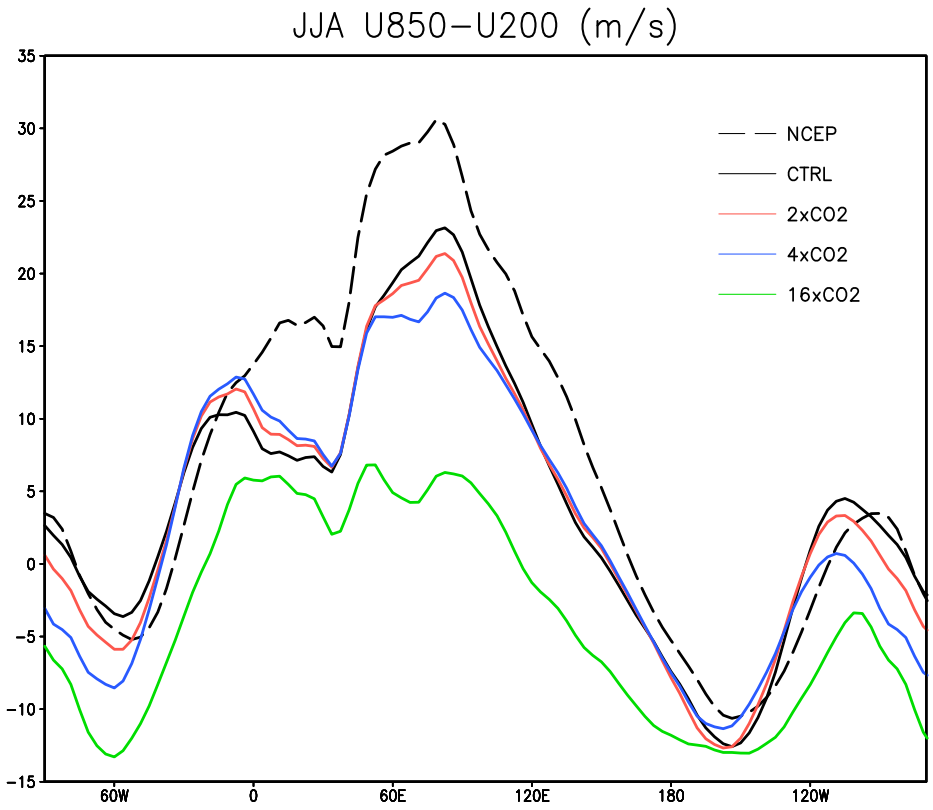

Fig. 2. Mean JJA U850-U200 (m/s) averaged between 5°S-15°N for NCEP winds (dashed black line), CTRL (solid black line), 2xCO2 (red line), 4xCO2 (blue line) and 16xCO2 (green line) experiments.

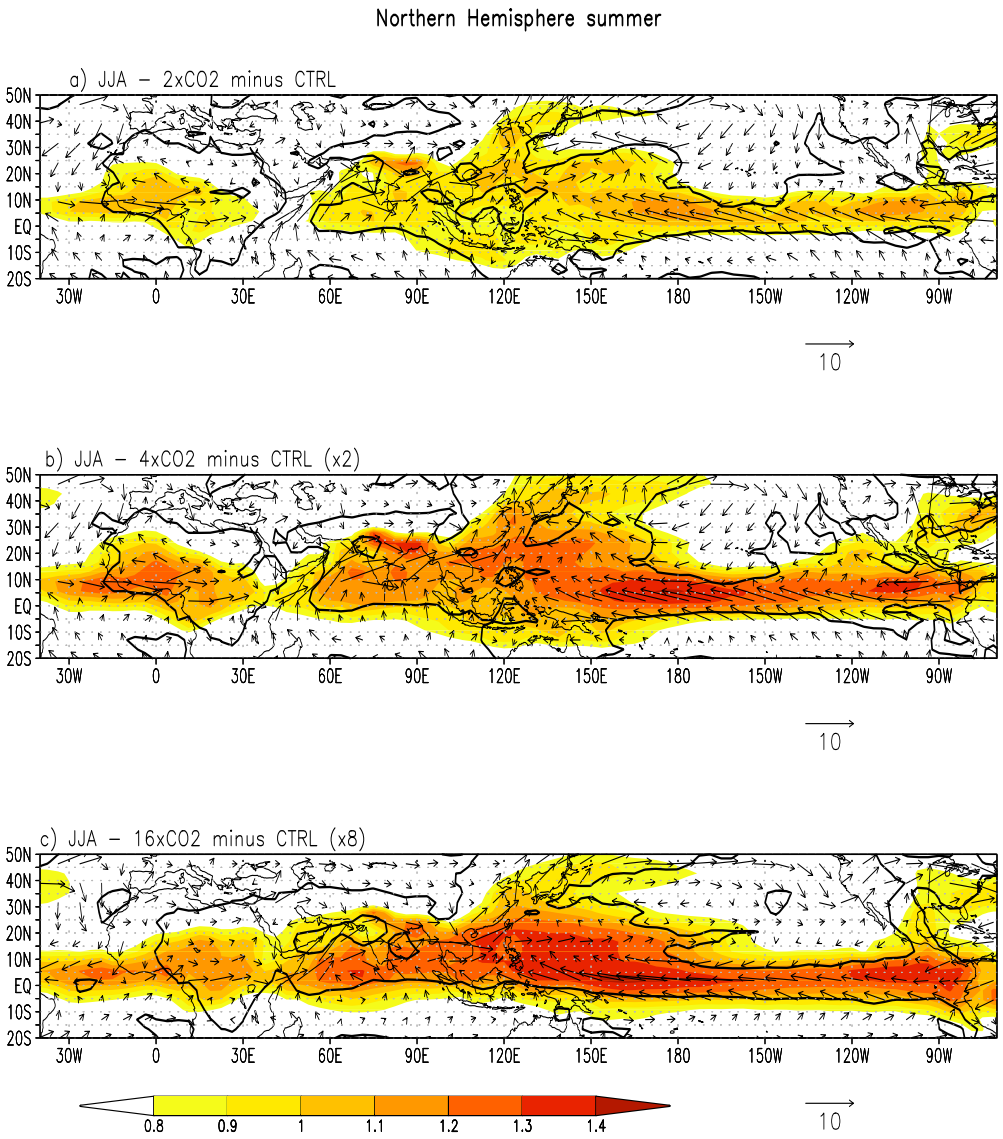

Fig. 3. JJA mean tropospheric vertically integrated specific humidity (kg/m^2, shaded) and water vapor flux (kg m^{-1} s^{-1}, vectors) differences from CTRL for (a) 2xCO2, (b) 4xCO2 and (c) 16xCO2 experiments. To maintain a unique vector length and a unique palette for all the experiments, the values of 4xCO2 and 16xCO2 cases have been divided by 2 and 8, respectively. The thick black solid line is the zero-contour difference of summer mean precipitation between CO_2 experiments and CTRL.

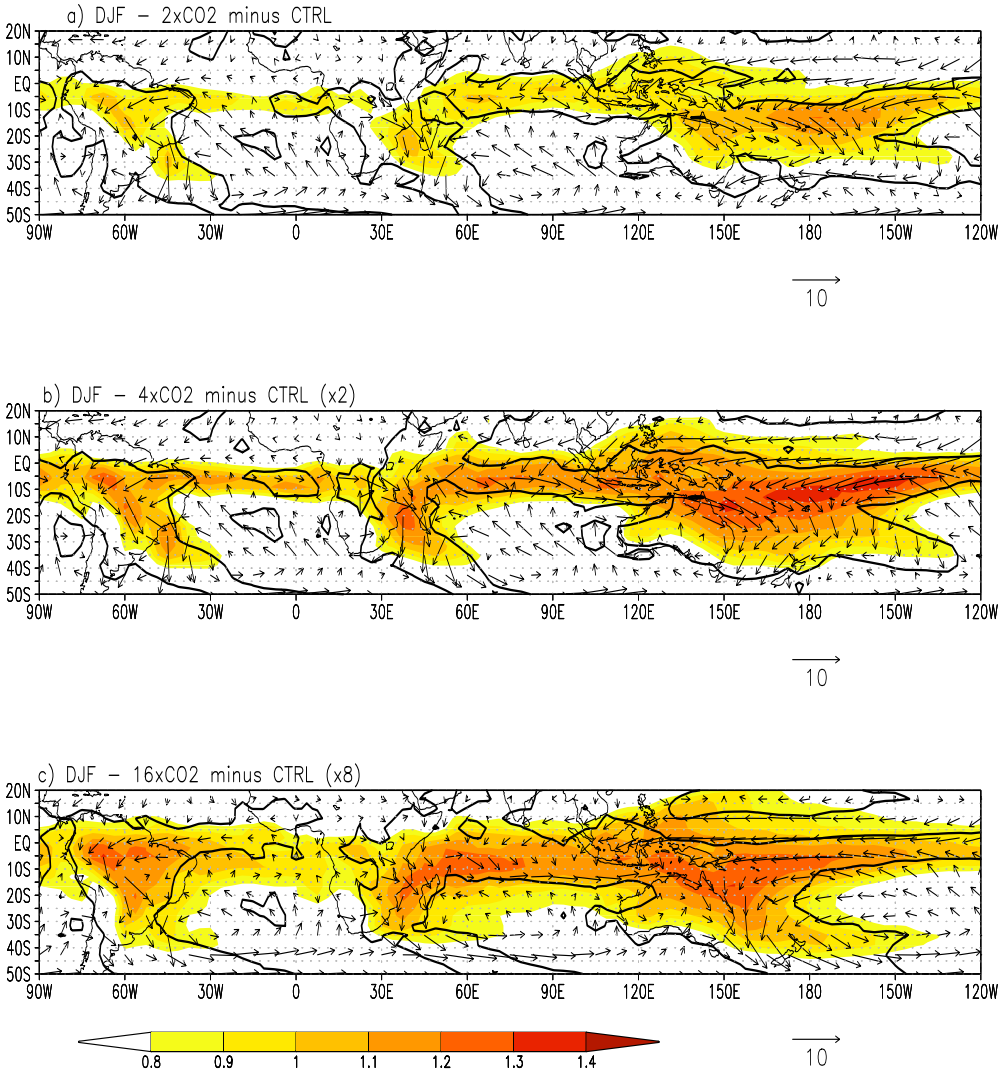

Fig. 4. Same as fig. 3 but for DJF.

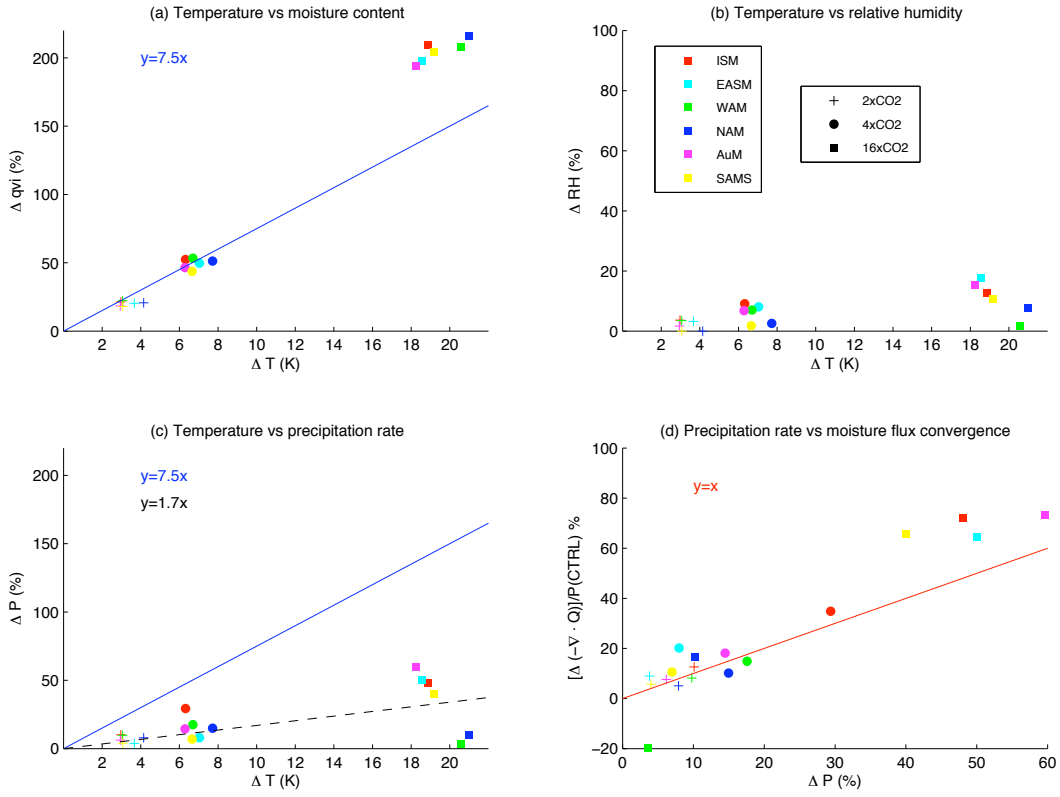

Fig. 5. Scatter plots of atmospheric temperature (T) differences versus (a) vertically integrated atmospheric water vapor content (qvi), (b) relative humidity (RH), (c) precipitation rate (P) anomalous percentages of 2xCO2 (crosses), 4xCO2 (filled circles) and 16xCO2 (filled squares) from CTRL in the different monsoon domains (red for ISM, cyan for EASM, green for WAM, blue for NAM, magenta for AuM, yellow for SAMS, black for SAfM). (d) is the scatter plot of precipitation anomalous percentages (ΔP), computed as described above, versus moisture flux convergence differences weighted on the precipitation of the CTRL ($\Delta(-\nabla \cdot Q)/P(CTRL)$ %). The solid blue line in panels (a) and (c) corresponds to a 7.5% increase per 1K warming, the dark dashed line in panel (c) corresponds to 1.7% increase per 1 K warming and the red line in panel (d) is y=x.

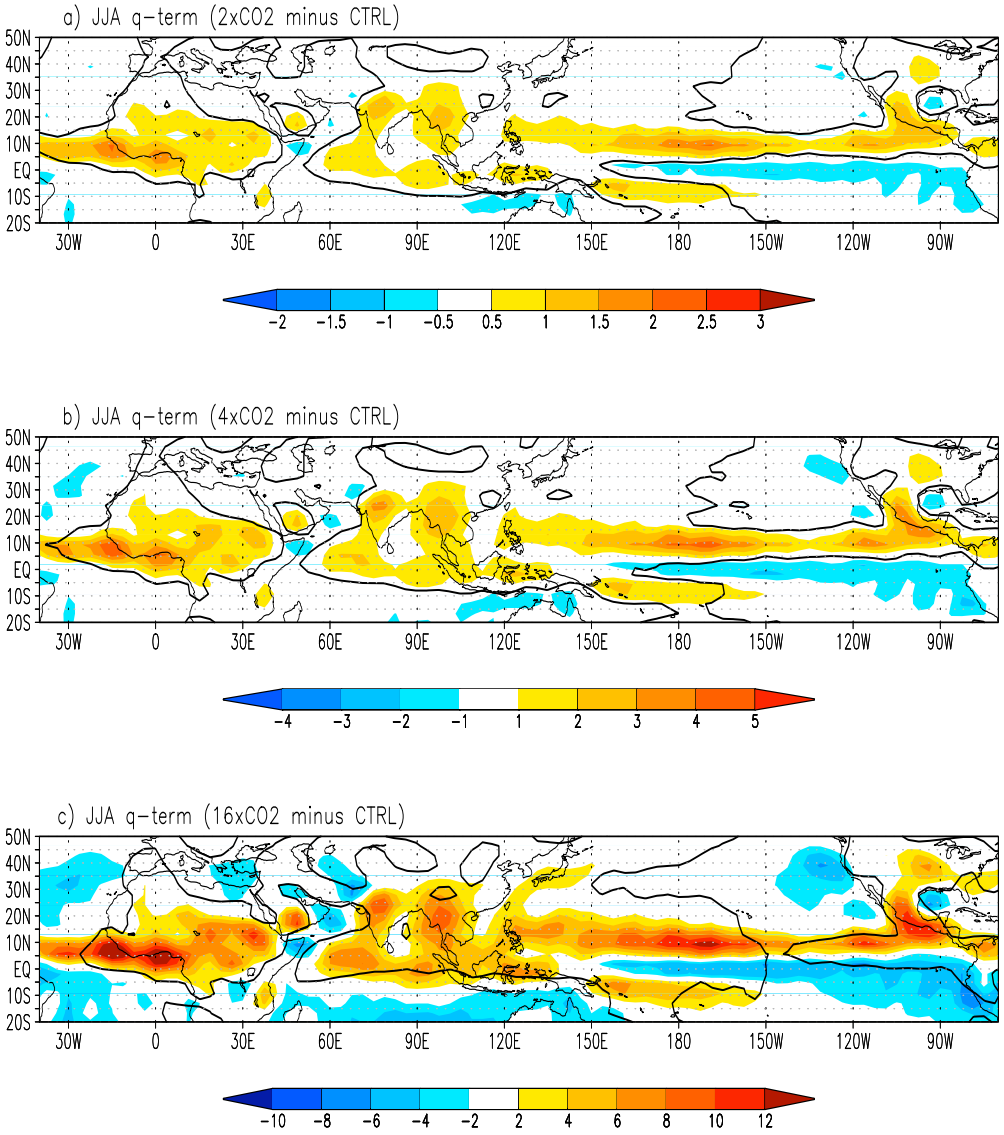

Fig. 6. JJA q-term ($-\langle\overline{\omega}\partial_p q'\rangle$, mm/day) for (a) 2xCO2, (b) 4xCO2 and (c) 16xCO2 experiments with respect to CTRL. The thick solid line is the zero-contour of the summer mean vertical velocity at 500 mb, and it is used to delimit the convergence zones.

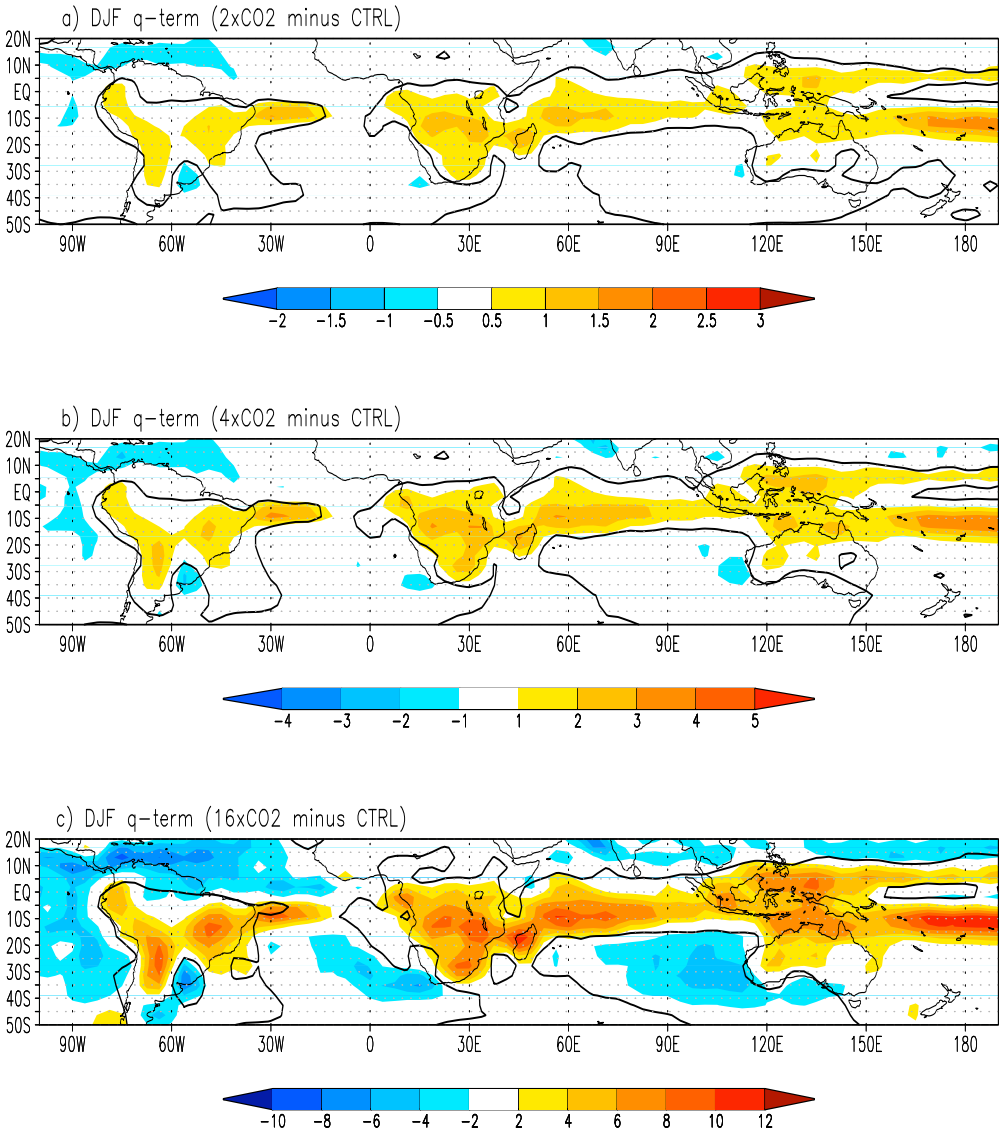

Fig. 7. Same as fig. 6 but for DJF.

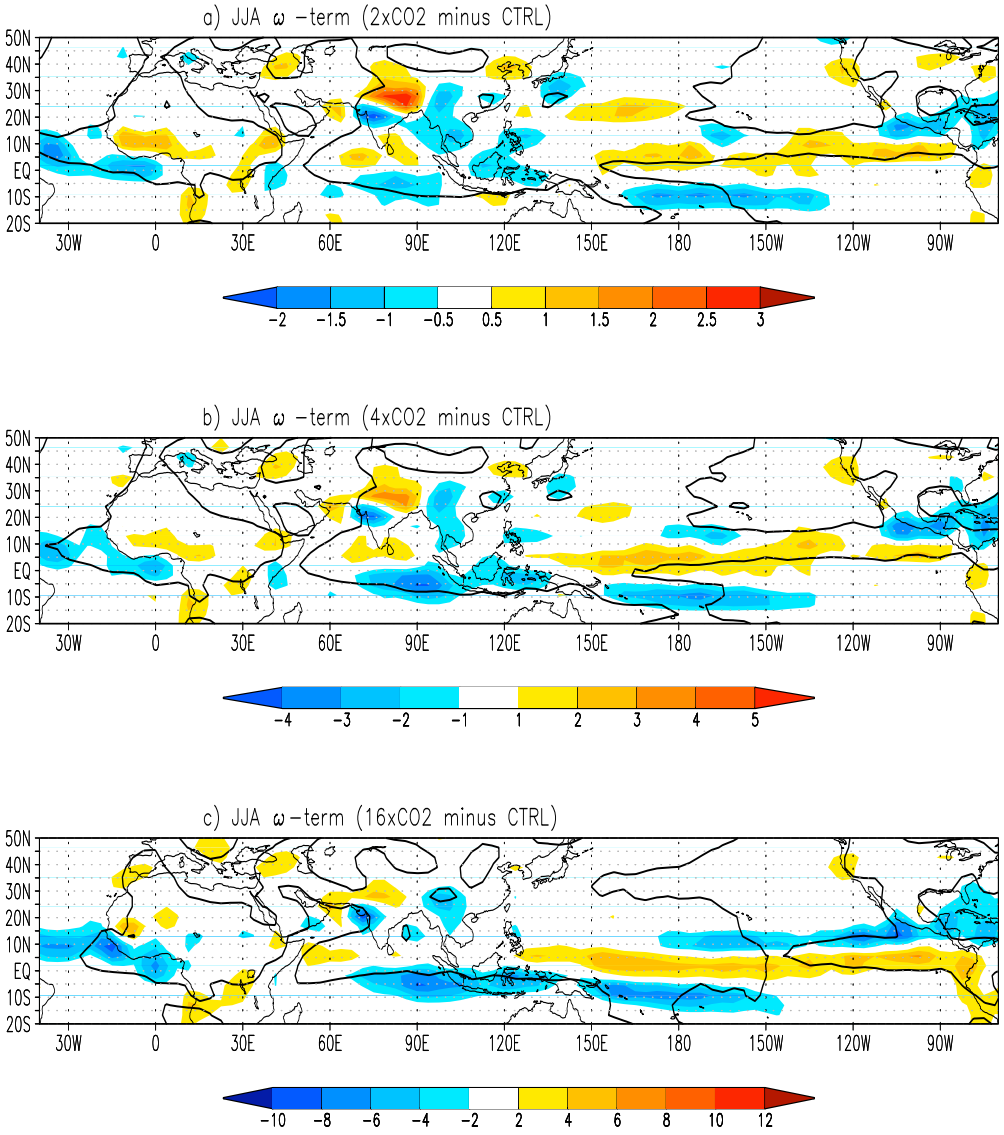

Fig. 8. JJA ω-term ($-\langle\omega^{'}\partial_p\overline{q}\rangle$, mm/day) for (a) 2xCO2, (b) 4xCO2 and (c) 16xCO2 experiments with respect to CTRL. The thick solid line is the zero-contour of the summer mean vertical velocity at 500 mb, and it is used to delimit the convergence zones.

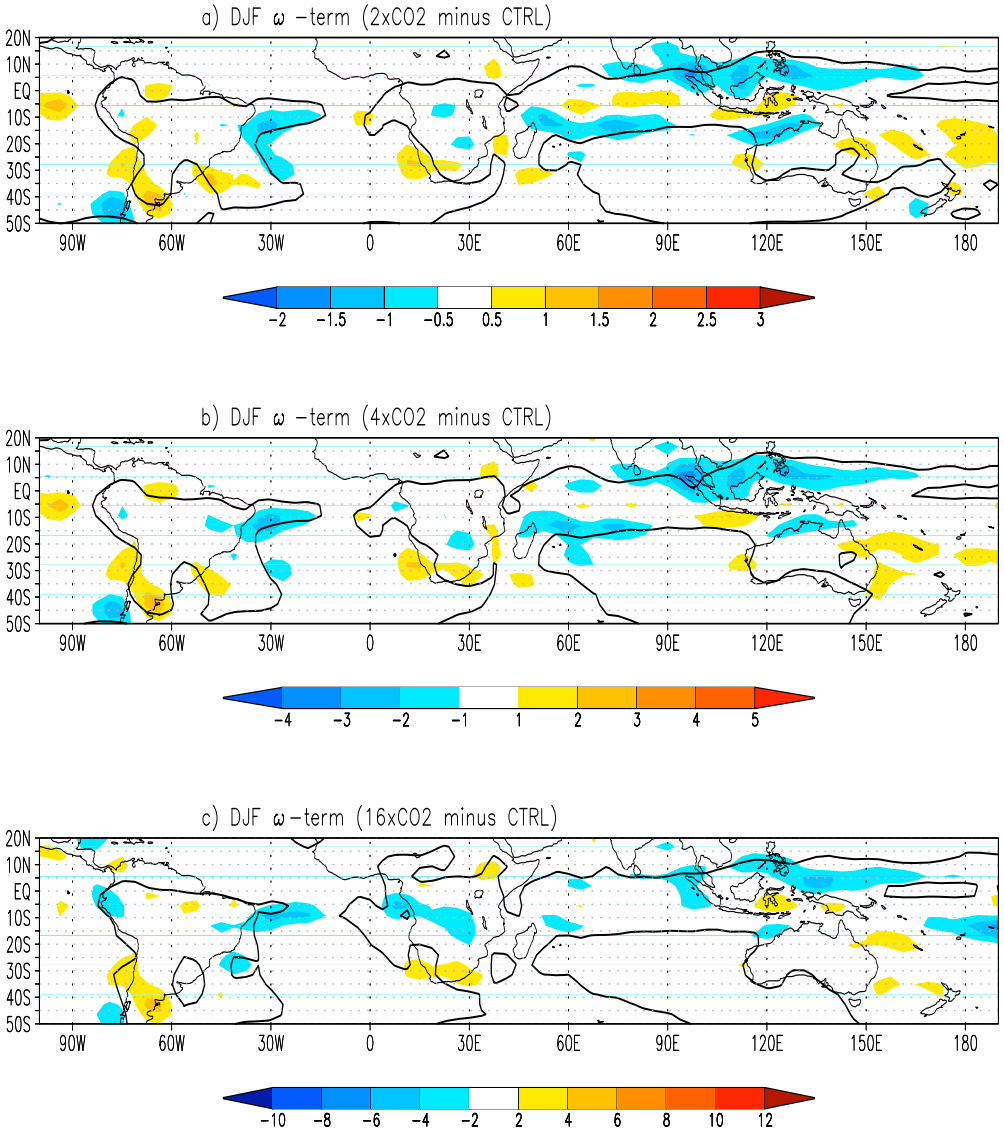

Fig. 9. Same as fig. 8 but for DJF.

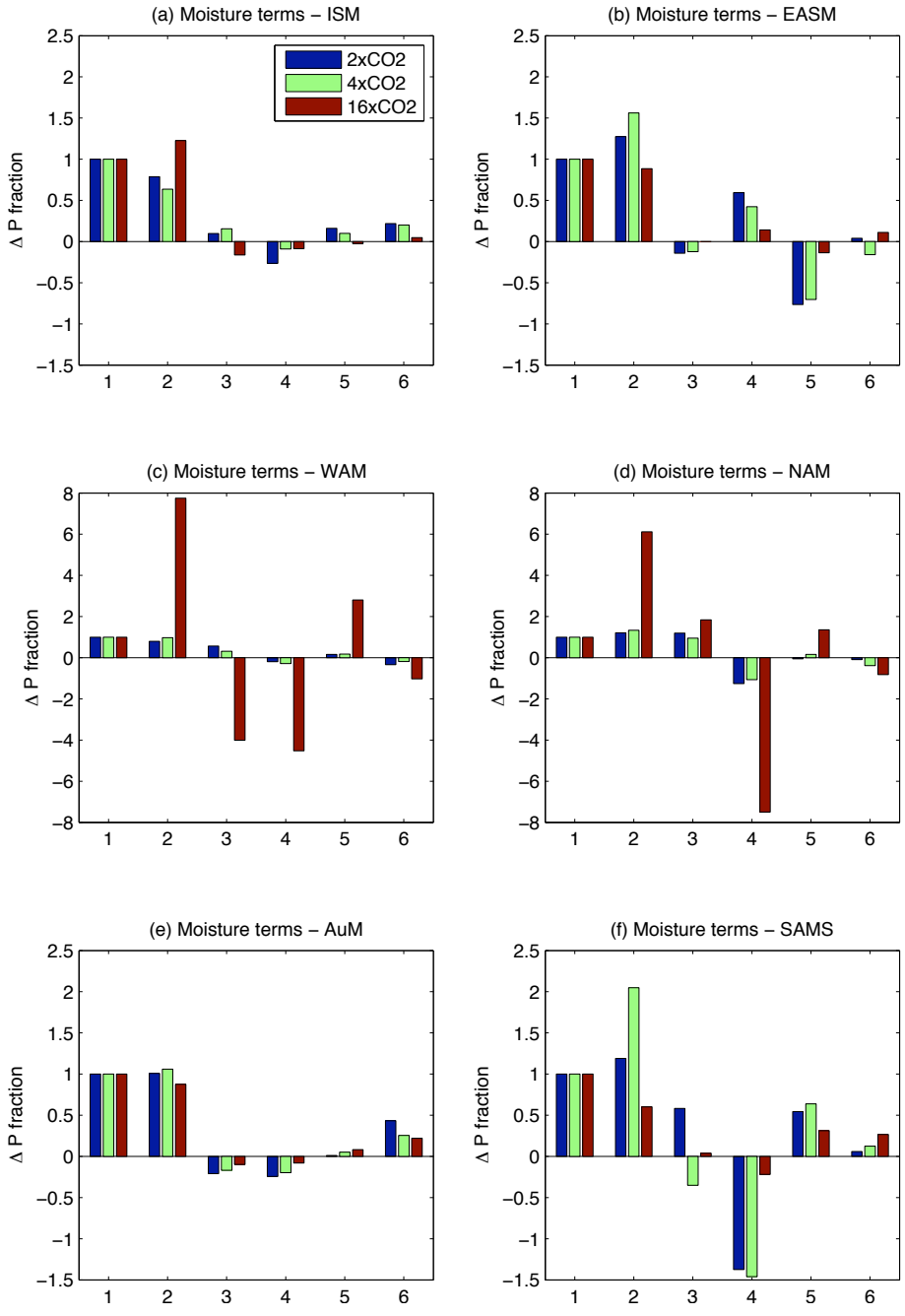

Fig. 10. Moisture terms of equation 2 expressed as fraction of P' for each monsoon domain as 2xCO2 (blue), 4xCO2 (green) and 16xCO2 (dark red) differences from CTRL. The terms shown are 1 - precipitation difference (P'), 2 - q-term ($-<\overline{\omega}\partial_p q'>$), 3 - ω-term ($-<\omega'\partial_p\overline{q}>$), 4 - advection term ($-<v\cdot\nabla q>'$), 5 - evaporation change (E'), and 6 - residuals (q_{res}). Each term is averaged in the corresponding monsoon region (a) Indian subcontinent (ISM), (b) East Asia (EASM), (c) West Africa (WAM), (d) North America (NAM), (e) Northern Australia (AuM) and (f) South America (SAMS) following the details specified in table 1. The y-axis in (c) and (d) is larger than in the other cases.

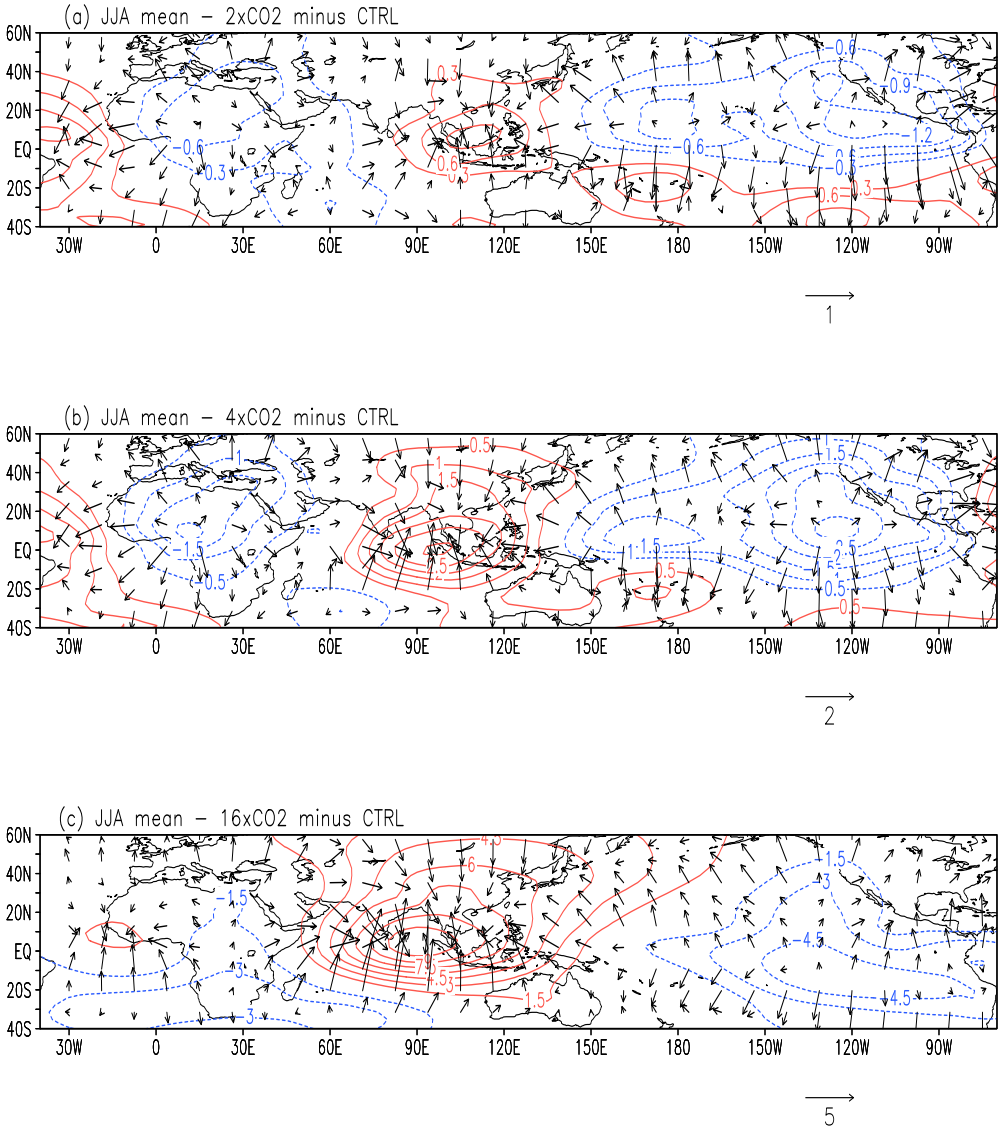

Fig. 11. Velocity potential ($10^6 m^2 s^{-1}$, contours) and divergent wind (vectors) at 200 mb as JJA mean differences of (a) 2xCO2, (b) 4xCO2 and (c) 16xCO2 experiment from CTRL. Positive (negative) values are in red (blue) solid (dashed) lines and contour interval is 0.3, 0.5 and 1 10^6 $m^2 s^{-1}$ in 2xCO2, 4xCO2 and 16xCO2 experiment, respectively.

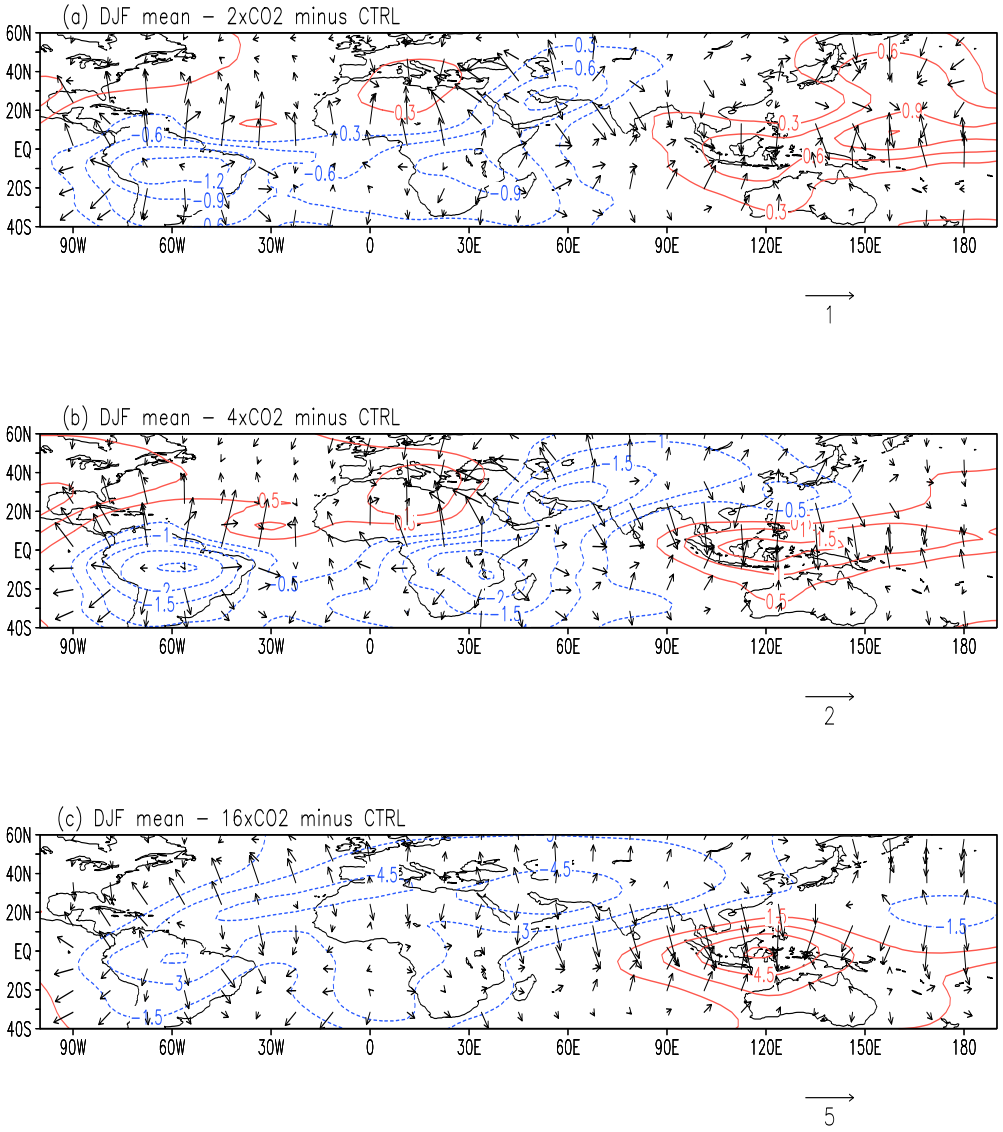

Fig. 12. Same as fig. 11, but for DJF.

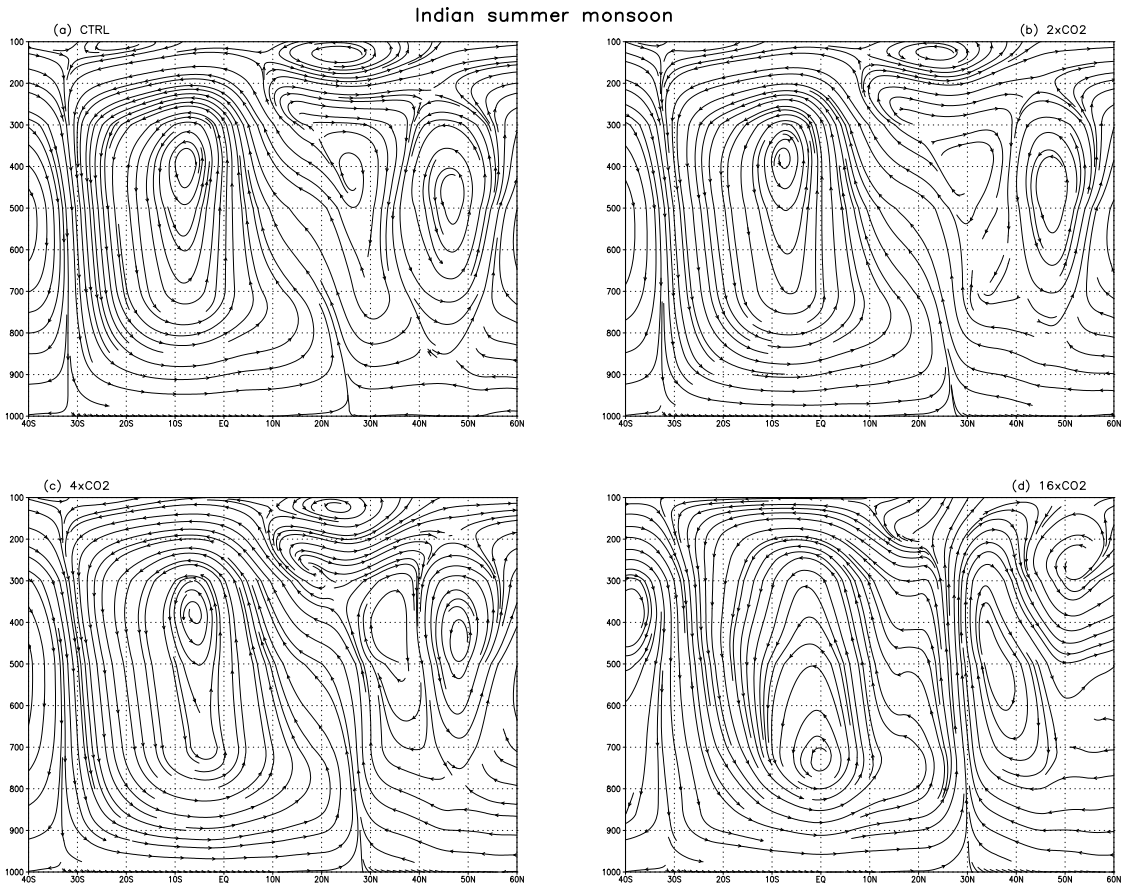

Fig. 13. Streamlines of divergent and vertical velocity over India for (a) CTRL, (b) 2xCO2, (c) 4xCO2 and (d) 16xC02 experiments.

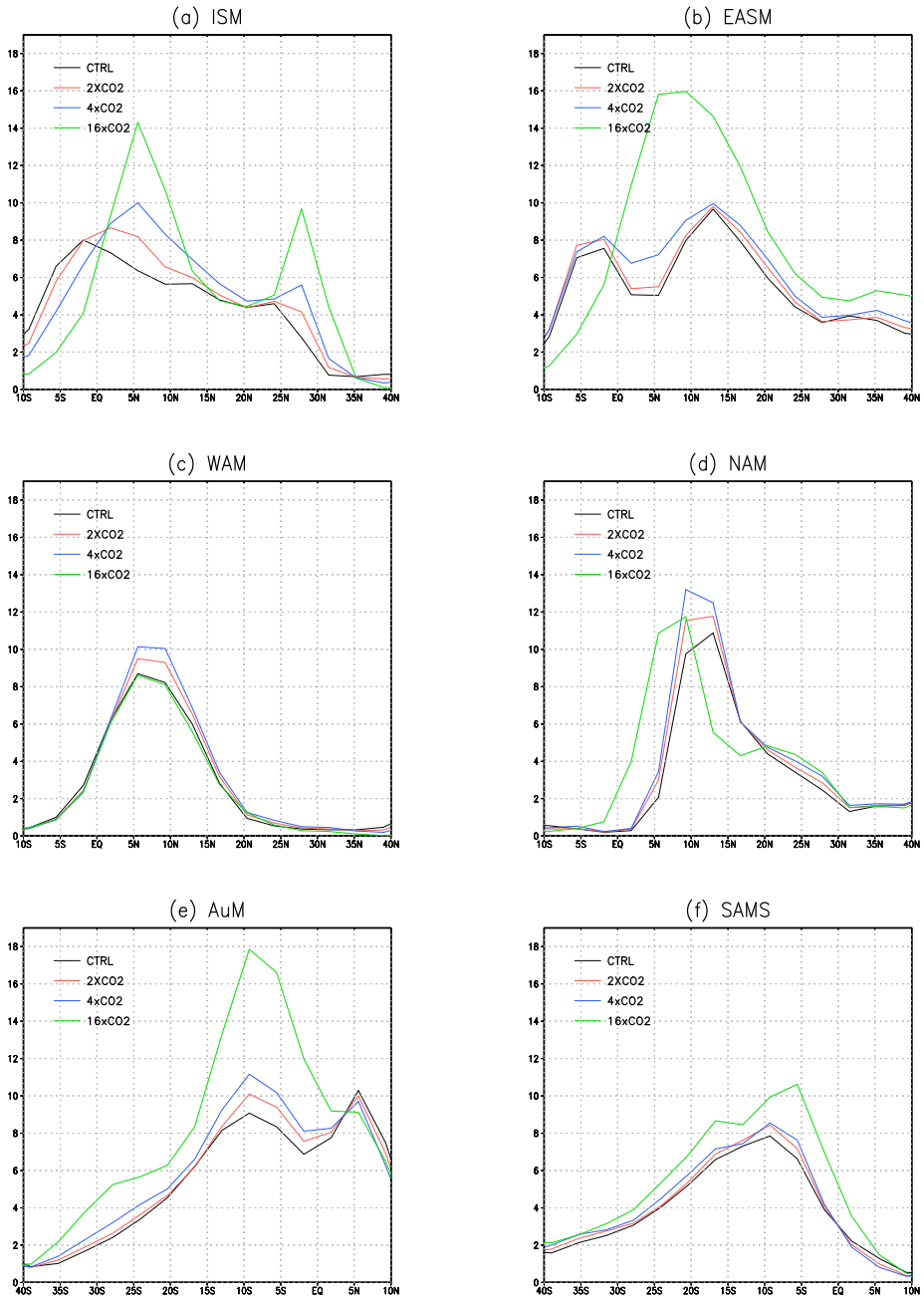

Fig. 14. Meridional profiles of summer mean rainfall (mm/day) zonally averaged over the monsoon areas of (a) ISM, (b) EASM, (c) WAM, (d) NAM, (e) AuM and (f) SAMS for CTRL (black), 2xCO2 (red), 4xCO2 (blue) and 16xCO2 (green) experiments.